JOURNAL OF GEOPHYSICAL RESEARCH, VOL. 102, NO. A12, PAGES 27,257-27,263, DECEMBER 1, 1997

Artificial auroral effects from a bare conducting tether

M. Martínez-Sanchez

Department of Aeronautics and Astronautics, Massachusetts Institute of Technology, Cambridge

J. R. Sanmartín

Escuela Técnica Superior de Ingenieros Aeronáuticos, Universidad Politécnica de Madrid, Madrid, Spain

Abstract. An electrically floating metallic bare tether in a low Earth orbit would be highly negative with respect to the ambient plasma over most of its length, and would be bombarded by ambient ions. This would liberate secondary electrons, which, after acceleration through the same voltage, would form a magnetically guided two-sided planar *e* beam, and result in auroral effects (ionization and light emission) upon impact on the atmospheric *E* layer, at about 120-140 km altitude. This paper examines in a preliminary way the feasibility of using this effect as an upper atmospheric probe. Ionization rates can reach up to 10^5 cm^{-3} s^{-1} if a tape, instead of a wire, is used as tether. Contrary to standard *e* beams, the beam from the tether is free of spacecraft charging and plasma interaction problems, and its energy flux varies across the cross section, which is quite large; this would make possible continuous observation from the satellite, with high resolution, both spectral and vertical, of the induced optical emissions. Ground observation might be possible at latitudes around 40°, for night, magnetically quiet conditions.

1. Introduction

The electrodynamic interaction of an orbiting conductive tether with geomagnetic field and ionosphere has received attention for potential applications ranging from ELF wave emission [*Grossi,* 1973] to power generation and propulsion [*Martínez-Sanchez and Hastings,* 1987]. The bottleneck is the efficient capture of ionospheric electrons at the anodic end of the tether: electron gyroradius and Debye length are so small compared to any useful, three-dimensional (3-D), passive anode that both magnetic guiding and electric shielding greatly reduce collection. This has motivated work on active contactors that create a plasma cloud to bridge the ionosphere [*Wilbur and Laupa,* 1988; *Gerver et al.,* 1990]. As a simple alternative, *Sanmartín et al.* [1993] proposed using uninsulated metallic tethers, whose anodic segment could collect electrons passively with no shielding or magnetic effects; this is the orbital-motion-limited (OML) regime of standard probe theory [*Chung et al.,* 1975], here applying because bare tether collection is a 2-D process governed by the thin tether cross section.

Actually, the OML regime in cylindrical geometry does not even require that the crosswise dimension be small compared to Debye length or gyroradius. An anodic segment in the kilometer range could lead to quite large (in addition to effective) collecting areas. A NASA experiment, Propulsive Small Expendable Deployment System (ProSEDS), will test bare tether collection in a 1999, Delta 2 flight; Marshall Space Flight Center is considering the use of bare tethers in the International Space Station, for reboost or peak power generation [*Johnson et al.,* 1996]. As a power generator, a bare tether would have a useful load and a cathodic contactor at its base, and electron collection, if optimal, would extend roughly to the upper 1/7 $\approx (m_e/m_i)^{1/5}$ of the total length (Figure 1). The remaining 6/7 of the tether would collect ions at a rate $\sqrt{m_e/m_i}$ times smaller for the same attracting bias.

Ions striking the metallic tether in Figure 1 would arrive with an energy that increases about linearly from the bias crossover point to the bottom. One consequence of this bombardment is the emission of secondary electrons, with a yield γ (electrons/ion) of a few per cent at low energies, and perhaps 20% at the 1 keV level. After acceleration by the tether-to-plasma local voltage, these electrons would constitute an *e* beam racing down the magnetic lines, much like those that are known to cause auroral displays at high latitudes. A convenient property of 2-D, OML collection (its independence from cross-section shape) would allow reaching high currents with light and flexible tethers; a 20 km long tether in low Earth orbit (LEO) orbit could yield a beam current of the order of 1 A, with electron energies of a few keV. We propose that measurements of photoemission rates induced by the well-defined electron flux from a bare tether, and comparison to detailed simulations, should make significant contributions to our knowledge of upper atmospheric kinetics and may uncover aeronomic mechanisms of importance in the thermosphere.

Auroral studies [*Jones,* 1974; *Kelley,* 1989; *Lysak,* 1993] have always been hampered by the difficulty in obtaining precise information about the characteristics of the naturally precipitating electrons. Natural auroral events occur at random times and vary rapidly and irregularly in space and time, which makes in situ observation with sounding rockets a chancy affair. Remote observation from overflying satellites has allowed very complete mapping of luminosities, but has yielded little correlating information on the energy, spectrum and pitch distribution of the originating electrons. This has led to active *e* beam experiments, with on-board beam sources

Paper number 97JA02044.
0148-0227/97/97JA-02044$09 00

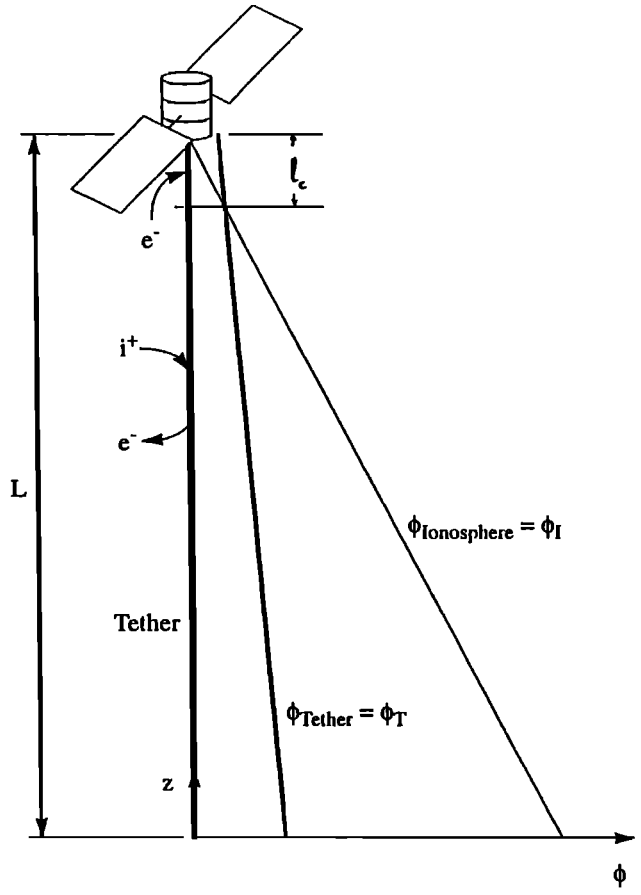

Figure 1. Potential diagram for a floating bare tether. An end mass at the bottom would make it dynamically stable, and would carry a diagnostics package.

that produce controlled artificial auroras. Ground observation may then further take advantage of the precise knowledge of both timing and location of the *e* beam.

Pioneer 1969 work with *e* beams [*Davis et al.*, 1971; *Hess et al.*, 1971] was followed by series of rocket experiments such as EXCEDE [*O'Neil et al.*, 1978a; *Paulsen et al.*, 1990], ECHO [*Israelson and Winckler*, 1975; *Arnoldy et al.*, 1985], or CHARGE [*Gilchrist et al.*, 1990; *Myers et al.*, 1990]. Beam sources have also been used on board the Shuttle. As compared with rockets, satellites allow repeated observations, and produce *e* beams originating well above the lower ionosphere, as in natural auroras. A difficulty found in almost all experiments, and particularly serious for satellites, was that beam firing affected the potential of the spacecraft, which serves as ground for the beam source itself.

The high energy flux involved leads to a second serious difficulty. The beam diameter is only twice the gyroradius at beam energy, or 10 m at 3 keV; for a representative 1 A current, the energy flux is 2 orders of magnitude above that for type 4 of natural auroras, for which type 1 is the weakest visible type. This compensates the small depth (~ 10 m) of the emitting layer in the direction of observation, compared with a depth ~ 10 km for an auroral arc, and leads to a similar brightness, making ground observations easy. On the other hand, intense beams are hard to predict; they produce suprathermal electrons [*Cartwright et al.*, 1978; *Banks et al.*, 1987] and plasma fluctuations [*Beghin et al.*, 1984; *Winckler et al.*, 1984] near the spacecraft, and are distorted by nonlinear plasma interactions [*Wilhelm et al.*, 1984; *Sasaki et al.*, 1985] that may structure the beam cross section [*Banks and Raitt*, 1988]. Most beam experiments have thus ended (whether originally so intended or not) studying beam physics and spacecraft charging, which are problems not quite related to auroral emissions.

By contrast, the tether beam source is entirely free of satellite-charging problems; as we shall see, no current flows at the ends of the tether. Also, the beam cross section is now about 10 m × 20 km, yielding an energy flux typically 10^3-10^4 times weaker than standard sources, well below any excitation or interaction thresholds [*Bernstein et al.*, 1979]. A drawback is that the resulting low brightness makes ground observation difficult. Brightness, however, would be much greater for observation from the spacecraft (which has the advantage of continuous recording). This is impracticable for a standard beam because of its very thin cross section, but a bare tether beam has one cross dimension of about 20 km, and the particle (and energy) flux varies from bottom to top of the tether, allowing for determination of volume emission rates by tomographic techniques.

In this paper we present a preliminary feasibility study for this concept. Section 2 reviews the electrodynamic aspects of the tether current generation, and section 3 discusses the beam characteristics. Section 4 presents a simplified model of the interaction of the electron beam with the upper atmosphere and gives ionization rates. Section 5 considers the observational options and their feasibility.

2. Tether Beam Emission

For this particular application, where we have no need for the tether as a generator, it is best to deactivate the cathodic contactor at the bottom; this makes both the tether electrically floating and the anodic segment shorter. In order to also reduce the high voltage exposure of the spacecraft, the tether should be deployed downward; Figure 1 shows a schematic of the configuration. The ionospheric potential in the vehicle's frame decreases upward at a rate $E = (\boldsymbol{v} \times \boldsymbol{B})_z$, where v is the orbital velocity and $\boldsymbol{B}$ the geomagnetic field. The tether supports only the small levels of current due to ion collection and will be regarded in a first approximation as being equipotential, floating at a positive potential $\Delta\phi_0$ with respect to the ionosphere at the upper end. The local voltage drop is then

$$\phi_T - \phi_I = \Delta\phi_0 - E(L - z). \tag{1}$$

In the OML regime the electron current collected per unit length of wire for large, positive bias is [*Chung et al.*, 1975; *Sanmartín et al.*, 1993]

$$\frac{dI_e}{dz} = e\, n_e \frac{p}{\pi} \sqrt{\frac{2e(\phi_T - \phi_I)}{m_e}}\ ; \tag{2}$$

for the region with $\phi_T < \phi_I$, ions are collected at a rate

$$\frac{dI_i}{dz} = e\, n_e \frac{p}{\pi} \sqrt{\frac{2e(\phi_I - \phi_T)}{m_i}}\ . \tag{3}$$

Here n_e is the ionospheric density, and p is the perimeter of the tether cross section. For an estimate of the crossover position we ignore the secondary electron emission and express the condition of zero net current collection by equating the integrals of (2) and (3) in their respective ranges. This yields

$l_c/L = \Delta\phi_0 / EL = (m_e/m_i)^{1/3}$, which is 0.032 for O^+ ions; since this is small, we will in what follows ignore the upper positive segment in Figure 1 and set $\Delta\phi_0 = 0$ in (1). An important property of the OML collection regime is that (2) and (3) are not restricted to circular wires, but apply to a general convex cross section [*Laframboise and Parker*, 1973].

The secondary emission of electrons by ion bombardment is characterized by a coefficient γ (electrons per ion) which (except at very low voltages) increases linearly with ion energy [*Cobine*, 1958]

$$\gamma = \gamma_1(\phi_1 - \phi_T) \approx \gamma_1 E(L - z), \tag{4}$$

typical values for γ_1 being 0.1 to 0.2 per kV. We can now multiply dI_i/dz in (3) times γ and integrate for the total secondary electron current,

$$I_{emit,T} = \frac{2\gamma_1}{5}\left(\frac{2e^3E^3}{m_i}\right)^{1/2} n_e \frac{p}{\pi} L^{5/2} = \frac{3}{5}\gamma_1 EL \times I_{i,T} \tag{5}$$

where $I_{i,T}$ is the total ion current and $(3/5)\gamma_1 EL$ is a mean emission coefficient. The vertical distribution of electron emission is given by

$$\frac{dI_{emit}}{dz} = -\frac{5}{2}\left(1 - \frac{z}{L}\right)^{3/2} \frac{I_{emit,T}}{L}. \tag{6}$$

As already noted, for the OML regime to hold, neither magnetic nor space-charge effects should affect particle collection. This puts limits on the dimensions of the tether cross section. For both power generation and thrust applications, where electron collection is the dominant process, magnetic effects, whose characteristic length is the thermal gyroradius, might place the strongest limitation. For the present application, however, we can totally ignore those effects because the ion gyroradius is larger than the electron gyroradius by the large factor $\sqrt{m_i/m_e}$. Space-charge effects then come into the fore; a preliminary estimate would allow a maximum crosswise "radius" of about twice a representative Debye length (~ 5.5 mm).

If we take E=175 V/km (an average value for 28°, 300 km orbits), $n_e = 3\times 10^{11}\text{m}^{-3}$ (nighttime level for an average solar activity at 300 km) and a 20 km long tape with $\gamma_1 = 0.15$ per kV and half-width 12 mm (perimeter ~ 48 mm), we calculate from (5) an emitted current of 0.63 A. By contrast, a circular wire emitting this current would be too rigid and heavy, having a 7.7 mm radius, and weighing about 9990 kg if made of aluminum, and over 3700 kg if made of a plastic material with a thin outer aluminum layer. This compares with 170 kg for a tape, say, 0.13 mm thick, for which the ohmic voltage drop would keep at 5% of the total emf, 3.5 kV. This advantage of tapes as regards weight reduction does not fully extend to other tether applications; using a tape reduces the length required to generate a given power but hardly modifies the power-to-mass ratio of the tether, which is bound by efficiency requirements on the circuit involving the tether.

Tethers 20 km long have been already successfully deployed on three occasions: Small Expendable Deployment System (SEDS) 1 and 2 were dielectric tethers flown on Delta 2 rockets in 1993 and 1994 respectively; TSS1-R, a conducting, insulated tether, was flown in the Shuttle in 1996. The danger of space debris hits, which increases with tether length, is negligible here because the tape is so wide; it would take 10 years for a severing hit [*Flury and Klinkrad*, 1994, Figure 11]. Possible tape twisting would have no effect on the 2-D ion collection process, because directional effects, either magnetic or from orbital motion, are absent; note in this respect that the relative orbital energy of oxygen ions, $\frac{1}{2}m_i v^2$ = 4.5 eV, is much less than the keV acceleration energies. Note also that although our tape might be too wide to ignore magnetic effects on electrons, thus breaking the OML law for electron collection (2), our results do not require a precise value for l_c/L (they just need it to be small).

3. Electron Beam Characteristics

The energy of the injected electrons, and hence the physics of their interaction with the atmosphere, is strongly influenced by the choice of (geographical) inclination i for the tether orbit. For a first approximation, the dipole model of the Earth's magnetic field is useful; the field at the magnetic equator is $B_0 \approx 3\times 10^{-5}$ T. One then finds that at a point in the orbit where the magnetic inclination is i_m, the induced electric field is

$$E = (\boldsymbol{v} \times \boldsymbol{B})_z = B_0 v \cos i_m, \tag{7}$$

which shows that to the extent that i_m can be considered constant during one orbit, the induced emf is also constant. The magnetic inclination, however, does vary on a daily basis with the angle β between the ascending node of the orbit and the magnetic pole meridian,

$$\cos i_m = \cos i \cos\alpha + \sin i \sin\alpha \sin\beta. \tag{8}$$

Here both i and the colatitude $\alpha \approx 11°$ of the magnetic pole are constant, i_m thus fluctuating daily between the limits $|i - \alpha|$ and $|i + \alpha|$. From (7), then, we obtain an emf centered at $B_0 v \times \cos i \cos\alpha$, which decreases with geographic inclination, and a superimposed daily oscillation between the limits $B_0 v \cos(i + \alpha)$ and $B_0 v \cos(i - \alpha)$.

Besides this simple variation, the irregularities of the actual geomagnetic field manifest themselves more or less strongly, depending on the area being overflown; especially prominent are the effects of the great negative magnetic anomaly over southern Africa, and of the positive Indo-Chinese anomaly. As an example of the complex intraorbital variations, the open circuit voltage of a 20 km tether at 300 km and i= 28.5° may reach as low as 1600 V [*Martínez-Sanchez and Hastings*, 1987, Figure 3], whereas the dipole model would yield a minimum voltage of 3470 V. We note, however, that the horizontal field is relatively smooth over the northern midlatitudes where most of the experimentation would be expected to take place. In those areas, the dipole approximation is reasonable; with this approximation, a 45° orbit still gives an emf between 2590 V and 3840 V, allowing a strong electron-atmosphere interaction, and covering most of the range of natural auroral electron energies.

The secondary electrons have low emission energies (a few eV) and accelerate away from the tether under the large potential difference $\phi_1 - \phi_T$ (a few kV). Note that the potential profile near the tether would be unaffected by space charge, for $e(\phi_1 - \phi_T)$ is very much larger than the thermal energy of ionospheric electrons (~ 0.15 eV), while the ratio of Debye length to tape half width is not small. The potential would then follow a 2-D Laplace (shallow) solution for some distance, most of the outward acceleration of secondary electrons occurring many centimeters away from the tape, where the potential is already nearly radial. For the approximate analysis of the next section we may thus assume that at the start of

their race along magnetic lines, secondary electrons are uniformly distributed in the azimuthal angle φ about the tether (Figure 2).

The pitch angle θ_p of these electrons would follow a (normalized) distribution $f_\infty(\theta_p) = (2/\pi)d\varphi/d\theta_p$, where the factor of 2 accounts for the fact that both φ and $-\varphi$ contribute to the same θ_p. The minimum pitch angle would be the magnetic dip angle I, and only the electrons moving down the field line are considered ($I < \theta_p < \pi/2$). From the relation $\cos\theta_P = \cos I \cos\varphi$ one obtains a fairly flat distribution,

$$f_\infty(\theta_p) = \frac{2}{\pi}\frac{\sin\theta_p}{\sqrt{\cos^2 I - \cos^2\theta_p}}. \qquad (9)$$

The dip angle I varies along each orbit between zero and a maximum (at the point nearest the magnetic pole) that is determined by the roughly constant magnetic inclination, $\tan I_{max} = 2 \tan i_m$, and ultimately again by the geographic inclination i as follows from (8).

The half width of the e beam perpendicular to the tether is taken to be the electron gyroradius $r_L(z)$ at the energy $\varepsilon_\infty(z) = eE(L - z)$. The one-sided flux of electrons (those moving down the magnetic tube) from a height z above the bottom of the tether is then, using (5) and (6),

$$\Phi_{e\infty}(z) = \frac{1}{2}\frac{|dI_{emit}/dz|}{2r_L e\cos I} = \frac{\gamma_1 EL}{4\pi\cos I}\sqrt{\frac{m_e}{m_i}}\left(1-\frac{z}{L}\right)n_e\Omega_e p, \qquad (10)$$

where Ω_e is the electron gyrofrequency; in the dipole approximation

$$\Omega_e(I) = \Omega_{e0}\sqrt{\frac{1+\tan^2 I}{1+\frac{1}{4}\tan^2 I}}, \qquad \Omega_{e0} \approx 5.3\times10^6 s^{-1}. \qquad (11)$$

Flux $\Phi_{e\infty}$ and energy ε_∞ are the basic characteristics of the e beam. The one-sided energy flux is

$$\Phi_{\varepsilon\infty}(z) = \Phi_{e\infty}(z)\varepsilon_\infty(z) = \Phi_{e\infty}(z)\times eEL(1 - z/L). \qquad (12)$$

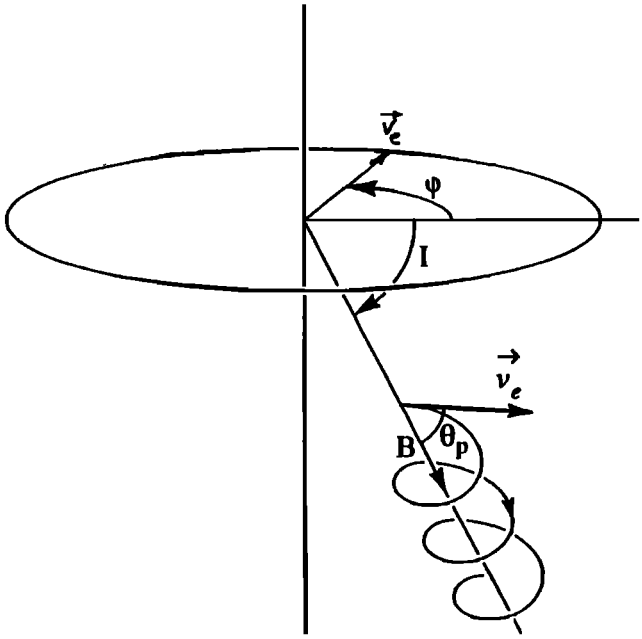

Figure 2. Geometry of tether electron emission and pitch determination.

Note that the beam characteristics are entirely determined by tether parameters L, p, and γ_1; plasma parameters n_e, m_i, I, and magnetic component perpendicular to orbit, E/v; and height z above the tether bottom.

4. Beam-Atmosphere Interaction

Most of the electron-atmosphere interaction will occur in the E layer, between 120 and 150 km altitude. This region is characterized by a predominance of molecular ions (O_2^+ and N_2^+ in particular), which recombine rapidly by dissociation after sunset. The nighttime ionospheric density at midlatitudes can reach as low as 10^2 cm^{-3} for very quiet magnetic conditions, while the daytime density is around 10^5 cm^{-3}, with some dependence on the sunspot cycle [*Kelley*, 1989]. By contrast, the F layer, where the tether itself would fly, is dominated by radiatively recombining O^+ ions (10^5-10^6 cm^{-3}) which survive the night with density reduction factors of only 2 to 4.

As beam electrons, now called "primaries", move in their helical paths down magnetic field lines, they are slowed down by a variety of inelastic interactions with air molecules. The most significant of those interactions is ionization, but for every ionizing event there are also a number of excitation collisions, followed mainly by prompt photon emission. One ionization is produced, on average, for every 35 eV of energy lost by the primary electron (the mean of 33 and 37 eV values for O_2 and N_2 respectively [*Rees*, 1989]); we denote this effective ionization energy as ε_i. For the moderate energies ε_∞ of interest, the bremmstrahlung loss is negligible [*Carlson and Egeland*, 1995] and beam broadening is negligible too, except at the lowest altitudes [*Davis et al.*, 1971; *Winckler*, 1980]. Also, the beam electron density is clearly too low for Coulomb collisions at the end of the beam range to count [*Martínez-Sanchez et al.*, 1992].

The ionization cross sections of N_2 and O_2 (summed over all ion states) are quite similar, and can each be approximated for energies above ~30 eV by

$$\sigma_i(\varepsilon) = \sigma_* g(\varepsilon/\varepsilon_*); \qquad g(u) \equiv \frac{u-1}{u^2}\ln u, \qquad (13)$$

with $\sigma_* = 9.7 \times 10^{-16}$ cm^2 and $\varepsilon_* = 23.6$ eV. The E layer atmosphere can be characterized by a linearly varying scale height for the total atmospheric density n; for the mean CIRA reference atmosphere we have a very simple, approximate law,

$$n(h) \approx 10^{31}/h^3, \qquad (14)$$

where h is altitude measured from 95 km above Earth's surface and 10^{31} is a dimensionless constant. As a primary electron with energy ε, pitch angle θ_p, and ionization mean free path $1/n\sigma_i$, advances a distance ds in its path, the altitude loss is $dh = -\sin I \cos\theta_p\, ds$, and the energy loss rate is

$$\sin I\cos\theta_p \frac{d\varepsilon}{dh} = \varepsilon_i\, n(h)\sigma_i(\varepsilon). \qquad (15)$$

For simplicity, we will consider two opposite rough models for pitch angle evolution, (1) electrons move at constant pitch angle, with a distribution frozen in its initial form $f_\infty(\theta_p)$, and (2) electrons reach an isotropic distribution (in the range $0 < \theta_p < \pi/2$) immediately after leaving the tether.

Starting with this last, simpler model we average (15) over θ_p and integrate from an initial energy $\varepsilon_\infty(z)$ at tether altitude

($h_\infty \approx \infty$) to obtain $\varepsilon\,[h, \varepsilon_\infty(z)]$. Making use of the small value of $1/ln(\varepsilon_\infty/\varepsilon_*)^2$, which is typically of order 10^{-1}, we find

$$1-\left(\frac{\varepsilon}{\varepsilon_\infty}\right)^2 \frac{ln(\varepsilon_\infty/\varepsilon_*)}{ln(\varepsilon/\varepsilon_*)} \approx \frac{10^{31}\sigma_*}{h^2}\frac{ln(\varepsilon_\infty/\varepsilon_*)^2-1}{<\mu_p>sinI} \times \frac{\varepsilon_i\varepsilon_*}{2\varepsilon_\infty^2} \equiv \frac{h_0^2(z)}{h^2}, \qquad (16)$$

where $<\mu_p> = 2/\pi$ is the average of $\mu_p \equiv cos\theta_p$, and h_0, as defined by the last equality, is the limit height for a vanishing ratio $\varepsilon/\varepsilon_\infty$. With beam spread ignored, we have $\Phi_e(h;z) = \Phi_{e\infty}(z)$ (and $\Phi_\varepsilon(h;z) = \Phi_{\varepsilon\infty}\,\varepsilon(h;z)$), the volumetric ionization rate then taking the simple form

$$\dot{n}_s\,(h;\,z) = \Phi_{e\infty}\,(z)\,n(h)\,\sigma_i[\varepsilon(h;\,z)]. \qquad (17)$$

Using (13), (14), and (16) in (17), for h not too close to h_0 (with $\varepsilon/\varepsilon_*$ still large), we find

$$\frac{\dot{n}_s}{\Phi_{e\infty}n(h_0)\sigma_i(\varepsilon_\infty)} = \frac{h_0^3/h^3}{\sqrt{1-h_0^2/h^2}}\left[1+\frac{\ln\sqrt{1-h_0^2/h^2}}{\ln(\varepsilon_\infty/\varepsilon_*)^2}\right]. \qquad (18)$$

For the column-integrated rate we find

$$\int_{h_0}^{h_\infty}\dot{n}_s dh = h_0\Phi_{e\infty}n(h_0)\sigma_i(\varepsilon_\infty)\left[1-\frac{1}{ln(\varepsilon_\infty/\varepsilon_*)^2}\right] \rightarrow <\mu_p>sinI\frac{\Phi_{\varepsilon\infty}}{\varepsilon_i}. \qquad (19)$$

The last form of (19) can be directly obtained from (15) and (17). Note that values $\varepsilon/\varepsilon_* = O(1)$ in (16) occur in an altitude range $h \approx h_0$, which is too narrow to make a sensible contribution to (19). The maximum rate occurs in this range, where $\dot{n}_s \approx \Phi_{e\infty}(z)\,n(h_0)\sigma_i(\varepsilon)$; we find

$$\dot{n}_{s\,max} = \Phi_{e\infty}(z)\,n(h_0)\sigma_*\,g_{max}, \quad g_{max} \approx 0.26 \qquad (20)$$

with $\sigma_i = \sigma_{imax} \approx 2.5 \times 10^{-16}\ cm^2$ at $\varepsilon \approx 4.24\varepsilon_* \sim 100$ eV [*Rees*, 1989, Appendix A4].

For the model with a frozen distribution $f_\infty(\theta_p)$, equation (16), with the average $<\mu_p>$ replaced by each value μ_p and h_0^2 replaced by $h_0^2\,<\mu_p>/\mu_p$, determines the energy $\varepsilon(h\sqrt{\mu_p})$ of a primary of pitch θ_p at altitude h; electrons with θ_p close to $\pi/2$ will lose all their energy at high altitudes, while those with θ_p close to I will penetrate most. Since (16) can also be viewed as a relationship between ε and θ_p at a given altitude, the volumetric ionization rate is still given by (17) except for the replacement

$$\sigma_i\left[\varepsilon(h;z)\right] \rightarrow \int_I^{\theta_{pmax}} d\theta_p f_\infty(\theta_p)\sigma_i\left[\varepsilon\left(h\sqrt{cos\theta_p};z\right)\right]; \qquad (21)$$

maximum energy corresponds to the minimum pitch, I, and maximum pitch, θ_{pmax}, corresponds to those electrons that have lost almost all their energy above h [$(\varepsilon/\varepsilon_\infty \le \varepsilon_i/\varepsilon_\infty \approx 0$, $\mu_{pmin}(h;z) \equiv <\mu_p>h_0^2/h^2$]. We find, instead of (18),

$$\frac{\dot{n}_s}{\Phi_{e\infty}n(h)\sigma_i(\varepsilon_\infty)} \approx \int_{\mu_{pmin}}^{\mu_I}\frac{2}{\pi}\frac{d\mu_p}{\sqrt{\mu_I^2-\mu_p^2}}\sqrt{\frac{\mu_p}{\mu_p-\mu_{pmin}}} \times\left[1+\frac{ln\sqrt{1-\mu_{pmin}/\mu_p}}{ln(\varepsilon_\infty/\varepsilon_*)^2}\right]. \qquad (18')$$

From $h_0\sqrt{<\mu_p>/\mu_I}$ to h_∞ we find a column-integrated rate that is μ_I times the previous result (19). The maximum rate, on the other hand, differs markedly from result (20) for the isotropic θ_p model. The integral in (18') ranges from 1 for $\mu_{pmin} = 0$, at $h \approx \infty$, to a value close to $\sqrt{2}$ for μ_{pmin} near μ_I, at $h \approx h_0\sqrt{<\mu_p>/\mu_I}$. The maximum rate is here smaller than (20) by the factor $[2\mu_I^3/<\mu_p>^3]^{1/2}\sigma_i(\varepsilon_\infty)/\sigma_{imax}$; also, the rate profile is rounder.

As an example of application for conditions of interest to our experiment, consider emission from near the lower end of the tether introduced in section 2 ($z/L \approx 0$, $L = 20$ km, $p = 48.3$ mm, $\gamma_I = 0.15$/kV), for $I = 45°$, $E = 160$ V/km, and 3×10^{11} O^+ ions per m^3. Equations (10)-(12) then give $\Phi_{e\infty} \approx 3.1 \times 10^{13}\ m^{-2}s^{-1}$, $\varepsilon_\infty = 3.2$ keV and $\Phi_{\varepsilon\infty} \approx 15.8$ ergs $cm^{-2}\,s^{-1}$ (intermediate between types 2 and 3). From (16) we find $h_0 \approx 27.7$ km and $h_0\sqrt{<\mu_p>/\mu_I} \approx 26.3$ km, absorption thus being complete at about 122 km above Earth's surface. Energy and maximum energy drop to 2.31 keV at $h = 1.5\ h_0$ and $h = 1.5 \times h_0\sqrt{<\mu_p>/\mu_I}$, in the θ_p isotropic and θ_p frozen models, respectively. In the first case, ionization rates (in units of $10^5\ cm^{-3}s^{-1}$) decrease from a maximum 3.6 at $h \approx h_0$ to 0.20 at $h = 1.5\ h_0$ with a representative average

$$\int_{h_0}^{h_\infty}\dot{n}_s dh/(2h_0/3) \approx 0.69;$$

the second model gives a 0.83 maximum and a 0.51 average (using $h_0\sqrt{<\mu_p>/\mu_I}$ instead of h_0).

5. Observational Considerations

In a steady state the background plus secondary electron population would be determined by the balance between beam-induced O_2, N_2 ionization, and the dissociative recombination of O_2^+ and NO^+ (since N_2^+ converts rapidly via $N_2^+ + O \rightarrow NO^+ + N$ [*Martínez-Sanchez et al.*, 1992]). The buildup time of the electron population, however, is much longer than the beam dwell time $\Delta t \approx 1.3\times10^{-3}$ s (10 m wide beam moving at 7.5 km/s). Thus the total plasma density will remain well below the steady state value, just changing from a background n_e to a modified value $n_e + \dot{n}_s\Delta t$. Although this might be twice the background density at heights with maximum ionization rates, in the case of very quiet magnetic conditions, it would be barely detectable.

Observations of auroral emissions from the excited E layer are likely to yield the most detailed picture of events, since prompt emission from excited states with typical lifetimes about 10^{-7} s can indeed build up to steady state levels in the dwell time; this excludes "forbidden" transitions such as the green line (557.7 nm) and the red doublet (630.0 and 636.4 nm) of atomic oxygen. Knowledge of the primary electron flux can be obtained from differential current readings at a few points along the tether, and careful preflight calibration of the emission coefficient γ versus ion energy for the material used. Use of measured values for n_e, m_i, and geomagnetic components in (10) and (12) might replace current readings. Direct magnetic perturbation measurements could also be performed, but it would be difficult to separate the electron currents emitted away from the tether from the basic wave-carried currents implied by the ion collection in the lower part of the tether and the electron collection in its upper part.

Ground observation could directly provide vertical resolution. The number of photons received at the detector per sec-

ond, from a part of the layer in Figure 3 with frontwidth $\Delta z/tan\ I$ and related to points on the tether in the range z, $z+\Delta z$, is

$$\Phi_D = \dot{n}_{em}\Delta H \frac{d}{\cos\alpha}\frac{\Delta z}{tanI}\frac{A_D}{4\pi\left(H/sin\alpha\right)^2} \qquad (22)$$

where $\dot{n}_{em}$ is the volumetric emission rate of photons of the type considered. Production rates of radiating species for natural auroras are reasonably well established [*Jones*, 1974]. A standard observed emission is that of the N_2^+ first negative band (427.8 nm); for this transition, *Jones* [1974, Figure 4.24] shows a peak emission rate of about 70 $cm^{-3}s^{-1}$ per erg cm^{-2} s^{-1} primary flux, yielding 1.12×10^3 cm^{-3} s^{-1} for the flux of our previous example, $\Phi_{e\infty} \approx 16$ erg $cm^{-2}s^{-1}$. A direct rate relation, $\dot{n}_{em}$ (427.8 nm)/ $\dot{n}_s \approx 1.75$ [*Carlson and Egeland*, 1995] yields the same emission rate at $\dot{n}_s = 0.84\times10^5$ cm^{-3} s^{-1} (compared with $\dot{n}_s$ values at the end of last section). If we wish to resolve $\Delta H = 1$ km, with $A_D = 100$ cm^2, $H = 125$ km, $\alpha = 45°$, $d = 10$ m, $I = 45°$, and $\Delta z = 1$ km at the bottom of our 20 km tether, we obtain from (22) a photon flux of 400/s for this line. The total photon count from all known observable transitions is about 50 times that for N_2^+ 427.8.

Detector feasibility depends on the surface brightness or luminosity of the source, as measured in Rayleighs ($4\pi/10^6$ times the number of photons per cm^2, per steradian, per second at the detector [*Jones*, 1974]). With this definition, (22) yields a luminosity

$$b(R) = \frac{1}{10^6}\dot{n}_{em}\left(\frac{d}{\cos\alpha}\right) \qquad (23)$$

with cgs units for $\dot{n}_{em}$ and d. For the N_2^+ 427.8 line and the other conditions of our example, we find $b \approx 1.6$ R; this is over 10^3 times weaker than a natural aurora of the same type, which has a much larger emitting depth. The UV N_2^+ transition at 391.4 nm has a yield 3 times greater [*Carlson and Egeland*, 1995], leading to $b \approx 5R$; luminosity calibration against bright stars would allow correcting for atmospheric extinction.

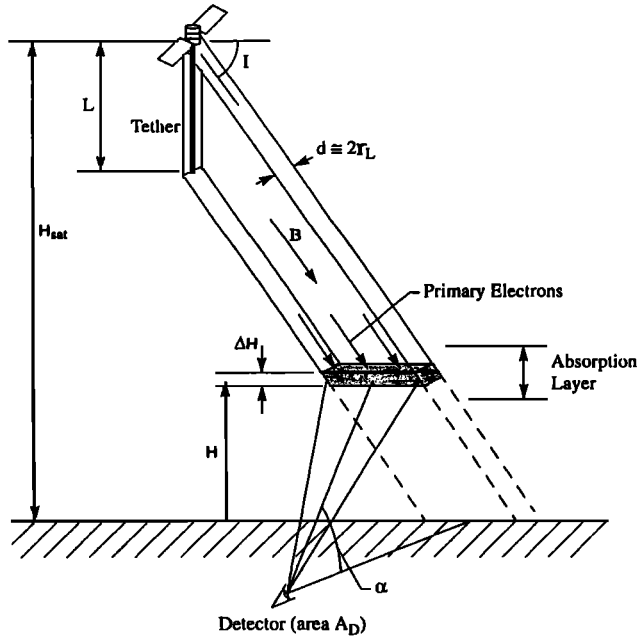

Figure 3. Geometry for ground observation of auroral emissions.

Brightness might be increased by observing at twilight, with the tether still illuminated and the lower atmosphere already dark; a day density $n_e \cong 10^6$ cm^{-3} would make b greater by a factor of 3. Somewhat larger values of tether dimensions L and p might be possibly allowed in (10) and (12), leading again to greater brightness. In any case, a luminous source of a few rayleighs might be detectable at latitudes around 40°, where the background energy flux of precipitating ions or electrons is only about 10^{-4} ergs $cm^{-2}s^{-1}$ under night, magnetically quiet conditions (*Kelley*, 1989, Fig. 5.27). At an elevation angle $\alpha = 45°$, the effective depth in (22) would be d~30 km, the height range of the auroral emission considered being about 30 km. The background luminosity would then be just 2% of the e beam luminosity of a tether with $\Phi_{e\infty} \approx 16$ ergs $cm^{-2}s^{-1}$.

Anyway, note that observation from the satellite, looking down the magnetic field, could result in greatly increased luminosities; photometers on board rockets emitting intense beams in the E layer have registered 10^7-10^8 R values [*O'Neil et al.*, 1978b]. A bare tether beam cross section is 20 km wide in the vertical plane containing the magnetic field, and maybe a few tens of meters thick (horizontally across) near the end of the beam range. Sweeping the line of sight through that plane, peak luminosities of 10^3-10^4 R should be reached. At emitting heights that lie 150 km below injection, the beam subtends an angle of about 4° at the satellite. A set of horizontal sweeps could then provide a brightness scan of line-integrated emission from electrons originating at different heights above the tether bottom, with varying energy fluxes. Note that for emission halfway up the tether, both $\Phi_{e\infty}$ and ε_∞ are reduced by 1/2, $\Phi_{e\infty}$ reduced by 1/4 , h_0 increased by about 2, and average ionization rates decreased by slightly less than 1/8; for the tether and conditions considered at the end of section 4, the average ionization rate decreases to values 0.095×10^5 and 0.071×10^5 cm^{-3} s^{-1}, in the isotropic θ_p and frozen θ_p models respectively.

Tomographic inversion of data would be required to obtain volume emission rates, as in the Visible Airglow Experiment on board the Atmospheric Explorer C satellite. An iterative relaxation algorithm should be used, a simple convolution procedure being unable to incorporate a priori information, as available on beam flux distribution. A convolution algorithm also makes for worse reconstruction when the set of line integrals is limited, as here [*Solomon et al.*, 1984; 1985]. A serious difficulty with iterative relaxation is backscattering of emitted light from both lower atmosphere and Earth's surface [*Hays and Anger*, 1978; *Abreu and Hays*, 1981]. This effect, however, is quite weak in our case because of the very small horizontal extent of the emitting region (a few tens of meters by 20 km); scattering models for diffuse aurora consider an emitting layer at a 110 km height, with infinite west-east extent and a 5° latitude width (~ 570 km).

6. Conclusions

Significant localized enhancements of ionospheric emission rates would result from the topside bombardment of the E layer by secondary electrons liberated by ions falling on a bare tether (a tape of some 20 km length, electrically floating in LEO orbit). As an e beam source a tether is free of the problems that have plagued standard sources. Continuous observation from the satellite, allowing for spectral and vertical resolution, has been shown to be feasible, and would, if correlated

with the incident e beam characteristics, yield important information on auroral processes. Ground observation might be also possible under limited conditions.

Acknowledgments. Fruitful comments from the referees are acknowledged. The work of J.R.Sanmartín was supported by DGYCIT (Spain) under grant PB94-0417-C03-01.

The Editor thanks A.D.Johnstone and another referee for their assistance in evaluating this paper.

References

Abreu, V.J., and P.B. Hays, Parallax and atmospheric scattering effects on the inversion of satellite auroral observation, *Appl.Opt., 20*, 2203, 1981.

Arnoldy, R.L., C. Pollock, and J.R. Winckler, The energization of electrons and ions by electron beams injected in the ionosphere, *J. Geophys. Res., 90*, 5197, 1985.

Banks, P.M., and W.J. Raitt, Observations of electron beam structure in space experiments, *J. Geophys. Res., 93*, 5811, 1988.

Banks, P.M., W.J. Raitt, P.R. Williamson, A.B. White, and R.I. Bush, Results from the vehicle charging and potential experiments on STS-3, *J. Spacecr. Rockets, 24*,138, 1987.

Beghin, C.J., J.P. Lebreton, B.N. Maehlum, P.I.J. Troim, and J.L. Michau, Phenomena induced by charged particle beams, *Science, 225*, 188, 1984.

Bernstein, W., H. Leinbach, P.J. Kellogg, S.J. Monson, and T. Hallinan, Further laboratory measurements of the beam plasma discharge, *J. Geophys. Res., 84*, 7271, 1979.

Carlson, H.C., and A. Egeland, The aurora and the auroral ionosphere, in *Introduction to Space Physics*, edited by M.G. Kivelson and C.T. Russell, Cambridge Univ. Press, pp.459-502, New York, 1995.

Cartwright, D.G., S.J. Monson, and P.J. Kellogg, Heating of the ambient ionosphere by an artificially injected electron beam, *J. Geophys. Res., 83*, 16, 1978.

Chung, P.M., L. Talbot, and K.J. Touryan, *Electric Probes in Stationary and Flowing Plasmas*, Springer-Verlag, New York, 1975.

Cobine, J.D., *Gaseous Conductors*, chap. V, Dover, New York, 1958.

Davis, T.N., T.J. Hallinan, G.D. Mead, J.M. Mead, M.C. Trichel, and W.N. Hess, Artificial aurora experiment: Ground-based optical observations, *J. Geophys. Res., 76*, 6082, 1971.

Flury, W., and H. Klinkrad, The space debris and meteoroid hazard for orbiting tethers, in *Proceedings, International Roundtable on Tethers in Space Eur. Space Agency Work. Prelim. Proc., WPP-081*, 528, 1994.

Gerver, M.J., D.E. Hastings, and M. Oberhardt, Theory of plasma contactors in ground-based experiments and in low Earth orbit, *J. Spacecr., 27*, 391, 1990.

Gilchrist, B.E., P.M. Banks, T. Neubert, P.R. Williamson, N.B. Myers, W.J. Raitt, and S. Sasaki, Electron collection enhancements arising from neutral gas jets on a charged vehicle in the ionosphere, *J. Geophys. Res., 95*, 2469, 1990.

Grossi, M.D., A ULF dipole antenna on a spaceborne platform of the PPEPL class, Letter Report on Contract NAS8-28303, NASA Marshall Space Flight Cent., Huntsville, Ala. May 1973.

Hays, P.B., and C.D. Anger, Influence of ground scattering on satellite auroral observations, *Appl. Opt., 17*, 1898, 1978.

Hess, W.N., M.C. Trichel, T.N. Davis, W.C. Beggs, G.E. Kraft, E. Stassinopoulos, and E.J.R. Maier, Artificial aurora experiment: Experiment and principal results, *J. Geophys. Res., 76*, 6067, 1971.

Israelson, G.A., and J.R. Winckler, Light production and electron scattering from electron beams artificially injected into the ionosphere, *J. Geophys. Res., 80*, 3709, 1975.

Johnson, L., J. Carroll, R. Estes, B. Gilchrist, E. Lorenzini, M. Martínez-Sanchez, J. Sanmartín, and I. Vas, Electrodynamic tethers for reboost of the international space station and spacecraft propulsion, paper presented at AIAA Space Programs and Technologies Conference, Am. Inst. of Aeronautics and Astronautics, Huntsville, Ala., Sept. 1996.

Jones, A.V., *Aurora*, D. Reidel, Norwell, Mass., 1974.

Kelley, M.C., *The Earth's Ionosphere*, Academic, San Diego, Calif., 1989.

Laframboise, J.G., and L.W. Parker, Probe design for orbit-limited current collection, *Phys. Fluids, 16*, 629, 1973.

Lysak, R.L., *Auroral Plasma Dynamics*, Geophys. Monogr. Ser., vol. 80, AGU, Washington, D. C., 1993.

Martinez-Sanchez, M., and D.E. Hastings, A systems study of a 100 kW electrodynamic tether, *J. Astronaut. Sci., 35*, 75, 1987.

Martinez-Sanchez, M., W.K. Cheng, D. Dvore, and M. Zahneiser, Electron energy distribution from intense electron beams in the upper mesophere and lower thermosphere, *J. Geophys. Res., 97*, 1363, 1992.

Myers, N.B., W.J. Raitt, A.B. White, P.M. Banks, B.E. Gilchrist, and S. Sasaki, Vehicle charging effects during electron beam emission from the CHARGE-2 experiment, *J. Spacecr. Rockets, 27*, 25, 1990.

O'Neil, R.R., F. Bien, D. Burt, J.A. Sandock, and J.A.T. Stair, Summarized results of the artificial auroral experiment, PRECEDE, *J. Geophys. Res., 83*, 3273, 1978a.

O'Neil, R.R., O. Sheperd, W.P. Reidy, J.W. Carpenter, T.N. Davis, D. Newell, J.C. Ulwick, and J.A.T. Stair, EXCEDE II test, an artificial auroral experiment: Ground-based optical measurements, *J. Geophys. Res., 83*, 3281, 1978b.

Paulsen, D.E., A.J. Ratkowski, F. Bien, L.C. Howlett, I.L. Thurgood, I.L. Kofsky, W. Boquist, and R.E. Murphy, EXCEDE III-Atmospheric excitation by electron deposition, *Eos Trans. AGU*, 71, 1500, 1990.

Rees, M.H., *Physics and Chemistry of the Upper Atmosphere*, Cambridge Univ. Press, New York, 1989.

Sanmartin, J.R., M. Martinez-Sanchez, and E. Ahedo, Bare wire anodes for electrodynamic tethers, *J. Propul. Power, 9*, 353, 1993.

Sasaki, S., et al., Ignition of beam plasma discharge in the electron beam experiment in space, *Geophys. Res. Lett., 12*, 647, 1985.

Solomon, S.C., P.B. Hays, and V.J. Abreu, Tomographic inversion of satellite photometry, *Appl. Opt., 23*, 3409, 1984.

Solomon, S.C., P.B. Hays, and V.J. Abreu, Tomographic inversion of satellite photometry. Part 2, *Appl. Opt., 24*, 4134, 1985.

Wilbur, P., and T. Laupa, Plasma contactor design for electrodynamic tether applications, *Adv. Space Res., 8*, 221, 1988.

Wilhelm, K., W. Stüdeman, and W. Riedler, Electron flux intensity distributions observed in response to particle beam emissions, *Science, 225*, 186, 1984.

Winckler, J.R., The application of artificial electron beams to magnetospheric research, *Rev. Geophys., 18*, 659, 1980.

Winckler, J.R., J.E. Steffen, P.R. Malcolm, K.N. Erickson, Y. Abe, and R.L. Swanson, Ion resonances and ELF wave production by an electron beam injected into the ionosphere: ECHO 6, *J. Geophys. Res., 89*, 7565, 1984.

M. Martínez-Sanchez, Department of Aeronautics and Astronautics, Massachusetts Institute of Technology, Cambridge, MA 02139. (email: mmart@mit.edu)

J. R. Sanmartin, Escuela Técnica Superior de Ingenieros Aeronáuticos, Universidad Politécnica de Madrid, 28040 Madrid, Spain. (email: jrs@faia.upm.es)

(Received February 6, 1997 ; revised June 19, 1997; accepted July 17, 1997.)